

Finding Rare AGN: X-ray Number Counts of *Chandra* Sources in Stripe 82

Stephanie M. LaMassa¹, C. Megan Urry¹, Eilat Glikman¹, Nico Cappelluti^{2,3}, Francesca Civano^{4,5}, Andrea Comastri², Ezequiel Treister⁶, Arifin⁷, Hans Böhringer⁸, Carie Cardamone⁹, Gayoung Chon⁸, Miranda Kephart¹, Stephen S. Murray^{10,11}, Gordon Richards¹², Nic Ross¹³, Joshua S. Rozner¹, Kevin Schawinski¹⁴

¹*Yale University*, ²*INAF - Osservatorio Astronomico di Bologna*, ³*University of Maryland Baltimore College*, ⁴*Harvard-Smithsonian Center for Astrophysics*, ⁵*Dartmouth College*, ⁶*Universidad de Concepción*, ⁷*National University of Singapore*, ⁸*Max-Planck-Institut Für Extraterrestrische Physik*, ⁹*Brown University*, ¹⁰*The Johns Hopkins University*, ¹¹*Harvard-Smithsonian Center for Astrophysics*, ¹²*Drexel University*, ¹³*Lawrence Berkeley National Lab*, ¹⁴*ETH Zürich*

ABSTRACT

We present the first results of a wide area X-ray survey within the Sloan Digital Sky Survey (SDSS) Stripe 82, a 300 deg² region of the sky with a substantial investment in multi-wavelength coverage. We analyzed archival *Chandra* observations that cover 7.5 deg² within Stripe 82 (“Stripe 82 ACX”), reaching 4.5 σ flux limits of 7.9×10^{-16} , 3.4×10^{-15} and 1.8×10^{-15} erg s⁻¹ cm⁻² in the soft (0.5-2 keV), hard (2-7 keV) and full (0.5-7 keV) bands, to find 774, 239 and 1118 X-ray sources, respectively. Three hundred twenty-one sources are detected only in the full band and 9 sources are detected solely in the soft band. Utilizing data products from the *Chandra* Source Catalog, we construct independent Log N -Log S relationships, detailing the number density of X-ray sources as a function of flux, which show general agreement with previous *Chandra* surveys. We compare the luminosity distribution of Stripe 82 ACX with the smaller, deeper CDF-S + E-CDFS surveys and with *Chandra*-COSMOS, illustrating the benefit of wide-area surveys in locating high luminosity AGN. We also investigate the differences and similarities of X-ray and optical selection to uncover obscured AGN in the local Universe. Finally, we estimate the population of AGN we expect to find with increased coverage of 100 deg² or 300 deg², which will provide unprecedented insight into the high redshift, high luminosity regime of black hole growth currently under-represented in X-ray surveys.

1. Introduction

Supermassive black holes (SMBHs) found in the centers of all massive galaxies grow by accreting matter, and are dubbed Active Galactic Nuclei (AGN) during this phase. X-rays are the most effective way to find moderate to high-luminosity AGN as they emit a significant fraction of their bolometric luminosity at these energies compared with inactive galaxies and nearly all X-ray point sources with $L_x > 10^{42}$ erg/s are AGN (e.g. Persic et al. 2004). (This dividing line misses low luminosity accreting black holes and can potentially include a few very energetic starburst galaxies that might attain these X-ray luminosities.) In particular, hard X-ray selection offers a nearly unbiased way to locate growing black holes (as long as the AGN is not obscured by Compton-thick or higher column densities, i.e. $N_H > 10^{24}$ cm $^{-2}$) since X-ray emission is generally transmitted through host galaxy levels of obscuration. Optical studies of the quasar luminosity function from large areas covered by the Sloan Digital Sky Survey (SDSS) have indicated that black hole growth evolves both as a function of luminosity and redshift (e.g., Richards et al. 2006), although these unobscured AGN likely represent only $\sim 30\%$ of the total black hole growth (e.g., Treister et al. 2009) or $\sim 50\%$ at lower luminosities (Reyes et al. 2008).

The deepest X-ray surveys to date have been successful in elucidating the low to moderate luminosity AGN population. The *Chandra* Deep Fields North and South (CDF-N and CDF-S) have peered to depths of 2 Ms and 4 Ms, reaching to 0.5-2 keV (2.0-8.0 keV) flux limits of 2.5×10^{-17} (1.4×10^{-16}) erg s $^{-1}$ cm $^{-2}$ and 9.1×10^{-18} (5.5×10^{-17}) erg s $^{-1}$ cm $^{-2}$ respectively, in CDF-N and CDF-S (Alexander et al. 2003; Xue et al. 2011). The Extended *Chandra* Deep Field South (ECDF-S) surrounded the original CDF-S survey, covering ~ 0.3 deg 2 with sensitivity limits of $\sim 1.1 \times 10^{-16}$ and $\sim 6.7 \times 10^{-16}$ erg cm $^{-2}$ s $^{-1}$ in the 0.5-2 keV and 2.0-8.0 keV bands, respectively (Lehmer et al. 2005). These observations are integral components of the larger multi-wavelength surveys of Great Observatories Origins Deep Survey (GOODS Giavalisco et al. 2004; Treister et al. 2004) and Multi-wavelength Survey by Yale-Chile (MUSYC Gawiser et al. 2006). *XMM-Newton* and *Chandra* have done deep surveys of the COSMOS field, reaching 0.5-2 keV fluxes down to 7×10^{-16} erg cm $^{-2}$ s $^{-1}$ on the whole field (Hasinger et al. 2007; Cappelluti et al. 2009) and 1.9×10^{-16} erg cm $^{-2}$ s $^{-1}$ in the inner area (Elvis et al. 2009; Civano et al. 2012), respectively. In the next two years, *Chandra* will survey the whole COSMOS field to reach the depth now only available in the central area (COSMOS Legacy, PI: F. Civano). However, since these surveys cover relatively small areas, high luminosity and/or high redshift AGN remain under-sampled compared with the population that would be uncovered in much wider areas. This means the existing census of black hole growth over cosmic time is incomplete. Indeed, the largest number of $z > 3$ X-ray selected AGN from a contiguous X-ray survey comes from *Chandra* observations of the Cosmic Evolution Survey (C-COSMOS, Elvis et al. 2009), with 81 such spectroscopically

confirmed AGN and an additional 20 sources with photometric redshift error distributions above $z = 3$ (Civano et al. 2011).

As high redshift and high luminosity sources are relatively rare, larger volume X-ray surveys are necessary to sample a representative population of growing black holes. So far, only XBoötes (9 deg², Murray et al. 2005; Kenter et al. 2005); ChaMP, a serendipitous survey based on archival *Chandra* data (10 deg², Kim et al. 2007a,b); extended ChaMP/SDSS (~ 32 deg², Green et al. 2009) and the *XMM-Newton* Large Scale Structure (XMM-LSS, ~ 11 deg², with a full survey coverage of 50 deg² planned, Pierre et al. 2004; Elyiv et al. 2012) surveys come close. Ancillary multi-wavelength data are then needed to provide additional critical information about these sources, such as an optical identification, with redshifts, to accurately calculate AGN and host galaxy properties like accretion luminosity, galaxy morphology, stellar content, star formation activity, galaxy mass, and so on. Follow-up spectroscopy over such large areas have been obtained only very slowly. About half of the X-ray sources in XBoötes have MMT Hectospec spectra as part of the AGN and Galaxy Evolution Survey (AGES, Kochanek et al. 2012), but this campaign took over 4 years. The optical follow-up for ChaMP also required a similar time investment (Trichas et al. 2012).

To efficiently probe the high luminosity and high redshift AGN population, we are beginning a large area X-ray survey in SDSS Stripe 82, a ~ 300 deg² area in a region of space which harbors substantial observational investments from an assortment of multiwavelength facilities, including FIRST and EVLA (radio, Becker et al. 1995; Hodge et al. 2011); Atacama Cosmology Telescope (millimeter, Das et al. 2011); UKIDSS and VISTA Hemisphere Survey (near-infrared, Lawrence et al. 2007; Emerson & Sutherland 2010) and GALEX (ultraviolet, Martin et al. 2005). Stripe 82 extends from $-60^\circ < \text{RA} < 60^\circ$ and $-1.25 < \text{Dec} < 1.25$, and is thus accessible from both hemispheres. An advantage of Stripe 82 over the full SDSS catalog, and by extensions the ChaMP/SDSS survey, is the increased optical depth: the imaging in Stripe 82 reaches two magnitudes deeper than any individual SDSS scan since any individual area was imaged ~ 80 times. The optical spectral density of Stripe 82 is also high thanks to observations with SDSS, 2dF and WiggleZ (Drinkwater et al. 2010) and continues to increase with spectroscopic campaigns from SDSS-III BOSS (Eisenstein et al. 2011) and AUS (Croom et al., in prep.): > 400 optical objects per square degree have spectra.

Combining archival *XMM-Newton* and *Chandra* observations as well as newly obtained *XMM-Newton* observations (which we will report in a future publication due to the detailed data reduction procedures required for these *XMM-Newton* data), the total X-ray coverage of Stripe 82 (Stripe 82 X) reaches ~ 20 deg² so far. Taking advantage of the high level of optical spectroscopic completeness, this survey will reveal more rare high luminosity ($L > 10^{44}$ erg s⁻¹) and high redshift ($z > 2$) AGN than previous X-ray surveys. Here, we

lay the foundation of this future analysis by reporting the X-ray source count numbers and general characteristics of the AGN found in Archival *Chandra* X-ray observations overlapping Stripe 82 (Stripe 82 ACX), covering a largely non-contiguous area of ~ 7.5 deg². Figure 1 illustrates the area covered as a function of survey flux limits in the 0.5-2keV, 2-8 keV and 0.5-8 keV bands for previous X-ray surveys and the archival *Chandra* observations in Stripe 82 presented here; these flux limits for comparison surveys represent the limits for on-axis pointings, so the depths becomes less sensitive by about an order of magnitude with increasing off axis distance. Throughout the paper, we use cosmology $H_0 = 70$ km/s/Mpc, $\Omega_M = 0.27$ and $\Lambda=0.73$.

2. Stripe 82 ACX: Archival *Chandra* Data

We utilized the *Chandra* Source Catalog (Evans et al. 2010) to identify X-ray sources and estimate the survey sensitivity of Stripe 82 ACX. The *Chandra* Source Catalog currently contains point and compact ($\leq 30''$) X-ray sources from the first eight years of public *Chandra* imaging observations, with associated data products, such as exposure maps, sensitivity maps, etc., reduced homogeneously. Full details of the data reprocessing are provided in Evans et al. (2010). In brief, all observations for the *Chandra* Source Catalog were recalibrated with a calibration database (CALDB) version created specifically for the *Chandra* Source Catalog. ACIS observations had the time-depended gain calibration applied and were corrected for CTI (CCD charge transfer inefficiency). The CIAO task *acis_run_hotpix* was run to remove pixel afterglow events, and bad pixels and hot pixels were flagged for removal. The background was screened to reduce the non X-ray background, removing intervals with strong background flaring.

Source detection was performed by the CIAO task *wavdetect*, with a limiting significance level of 2.5×10^{-7} , corresponding to ~ 1 false detection per pointing. For a source to be included in the *Chandra* Source Catalog, a conservative threshold was chosen to mitigate the inclusion of spurious detections as real sources: ~ 10 source photons (on-axis), or ~ 20 -30 source counts (off-axis), had to be detected in any individual band. This threshold is more conservative than that used in previous *Chandra* surveys (see Evans et al. 2010; Goulding et al. 2012, for a comparison). The *Chandra* Source Catalog estimates the uncertainty by S/σ_e , where $\sigma_e = FWHM/(2\sqrt{2\ln 2})$ and the FWHM is of the posterior probability density ($p(S|CB)$) for the flux (S) assuming that the total counts (C) and background counts (B) have a Poisson distribution. This flux threshold removes $\sim 1/3$ of the sources detected by *wavdetect*. We note that though a source is included in the catalog, this only ensures a significant detection in an individual band: this same source may have non-zero fluxes in

other bands, but those fluxes may not be significant at the 3σ level.

We use data from all ACIS-I and ACIS-S observations with exposure times of at least 5 ks for this analysis, totaling 95 individual *Chandra* pointings. The distribution of net exposure times for these observations is shown in Figure 2. A majority of pointings are at shallow depth, <20 ks, though a handful of much deeper observations do exist in this field. For comparison, we also plot the distribution of exposure times for ACIS observations greater than 5 ks in the *Chandra* Source Catalog that are not in the Stripe 82 field; this distribution is normalized by the number of sources in Stripe 82 to ease facilitate a direct comparison. As can be seen clearly in Figure 2, the shallow depth of the majority of the observations in Stripe 82 contrasts with the rest of the *Chandra* Source Catalog; a Kolmogorov-Smirnov test yields a negligible probability, $\sim 2 \times 10^{-10}$, that the two distributions are drawn from the same parent population. About 1/3 of the Stripe 82 pointings (i.e., 29 *Chandra* observations) are from the XDEEP2 survey with exposure times ≤ 10 ks; however, even after removing this subset of observations, the Stripe 82 coverage is still skewed to lower exposure times compared with the *Chandra* Source Catalog as a whole. As discussed in Section 2.2, the shorter exposure times results in a lower percentage of significant detection in the 2-7 keV band compared with the *Chandra* Source Catalog as a whole and previous X-ray surveys. Figure 3 shows the positions of the archival *Chandra* observations in Stripe 82. The two dense pointing regions at $RA = \sim 352^\circ$ and $RA = \sim 37^\circ$ are observations from the XDEEP2 survey, Fields 3 and 4, respectively (Goulding et al. 2012).

2.1. Survey Sensitivity

We estimated the Stripe 82 ACX survey sensitivity at the 4.5σ flux significance threshold, corresponding to less than 1 spurious source per 100 deg^2 *, by creating sensitivity maps for each observation in the soft (0.5-2 keV), hard (2-7 keV) and full (0.5-7 keV) bands.² First, exposure maps were created, where we used the level 3 event files from the *Chandra* Source Catalog and downloaded the aspect solution file, mask file and parameter block file from the *Chandra* archive; these level 3 event files are similar to the level 2 event files in-

*We estimated this number by noting that ~ 1500 unique sources were detected in the 7.5 deg^2 covered here and then extrapolating to a 100 deg^2 area.

²We note that the *Chandra* Source Catalog runs the source detection algorithm and provides products and fluxes in the more narrow “s” (0.5-1.2 keV) and “m” (1.2-2 keV) bands. For consistency with previous X-ray surveys, however, we explore the *Chandra* number counts in the traditional “soft” band, 0.5-2 keV. The hard and full bands defined here are consistent with those from the *Chandra* Source Catalog, i.e., only the “soft” band is redefined.

cluded in the *Chandra* data archive (i.e., filtered files suitable for data analysis), but with different good time interval (GTI) filters applied to remedy background flaring. We created aspect histograms for each active chip in an observation with CIAO tool *asphist*, using the aspect solution and event files as input. We then created an instrument map for each chip, which provides information about the effective area as a function of detector position, using the CIAO tool *mkinstmap*. As the effective area is a function of energy, we provided an input file of spectral weights derived from the CIAO routine *make_instmap_weights* using a power law model with $\Gamma = 1.4$, to be consistent with previous *Chandra* surveys to which we compare our number counts (i.e., ECDF-S, *Chandra*-COSMOS and ChaMP). *mkinstmap* was also given the mask file and parameter block file, which defines the clocking parameters for each pixel (i.e., how long the pixel is exposed before read-out). Using these instrument maps and aspect histograms, an exposure map for each chip is then created using CIAO tool *mkexpmap*. Finally, these individual chip by chip exposure maps are combined into one image with CIAO routine *reproject_image*, producing an exposure map for each observation in each band.

To create the sensitivity maps, we used the background images in the hard and full bands provided by the *Chandra* Source Catalog, with the narrow “s” and “m” bands added to produce a soft band background image. Using CIAO tool *mkpsfmap*, new PSF images were then generated at the spectral weighted mean energies of each band, i.e., 1.02 keV, 3.79 keV and 1.98 keV for the soft, hard and full bands, respectively, assuming a powerlaw with $\Gamma=1.4$. Finally sensitivity maps for each obsid were created from these exposure maps and PSF images, with CIAO tool *lim_sens*, using a 4.5σ flux threshold. These sensitivity maps were then converted from photon flux units to energy units using an absorbed power law model with $\Gamma = 1.4$ and $N_H = 3 \times 10^{20} \text{ cm}^{-2}$, the approximate absorption to our Galaxy within Stripe 82 (see Table 1 for conversion factors).

We effectively mask out the chip edges where source detection becomes improbable by “turning off” pixels where the exposure map drops below 15% of the maximum value. We note that no sources fall within these masked out pixels. To gauge full sensitivity across the survey, the individual sensitivity maps were overlaid on a grid of pixels spanning the Stripe 82 area. In overlapping regions, the most sensitive pixel (i.e., the lowest limiting flux) was chosen. From this Stripe 82 region sensitivity map, we then calculated the cumulative histogram of survey area as a function of limiting flux, producing the area-flux curves in Figure 4. Stripe 82 ACX covers $\sim 7.5 \text{ deg}^2$ of non-overlapping area. As noted in Table 1, the flux limits of this survey are $\sim 7.9 \times 10^{-16}$, $\sim 3.4 \times 10^{-15}$ and $1.8 \times 10^{-15} \text{ erg cm}^{-2} \text{ s}^{-1}$, with half the survey area visible to depths of $\sim 1.4 \times 10^{-14}$, $\sim 4.7 \times 10^{-14}$ and $\sim 2.8 \times 10^{-14} \text{ erg cm}^{-2} \text{ s}^{-1}$ in the soft, hard and full bands, respectively.

2.2. Source Selection

From the Source Observation Table in the *Chandra* Source Catalog, we isolated point sources lying in Stripe 82 that are not saturated, on the ACIS read-out streak or suffering from pile-up.³ For the hard and full bands, the aperture corrected flux in photon units was converted to energy units using the conversion factors listed in Table 1. To derive the soft flux, we had to ensure the “s” and “m” fluxes were combined with appropriate weights to match that of the sensitivity map. The aperture corrected net counts in the “s” (C_s) and “m” (C_m) bands from the *Chandra* Source Catalog were added, giving soft band counts (C_{soft}):

$$C_{soft} = C_s + C_m \quad (1)$$

These counts were then divided by the pixel from the soft band exposure map corresponding to the location where the source was detected (exp_{soft}), where the exposure map was created as described in Section 2.1:

$$F_{soft}^{ph} = C_{soft}/exp_{soft} \quad (2)$$

Again, the soft flux in photon units were converted to energy units via the conversion factor listed in Table 1.

To determine whether the detection is significant at the 4.5σ level, and for consistency with the area-flux curves from which we generate the LogN - LogS relationships, we compared the X-ray source list with the sensitivity maps: the source flux had to meet or exceed the limiting flux from the sensitivity map at the pixel where the source was identified in order for us to consider the source as significantly detected in that specific energy band. There were 271 sources detected in multiple observations (identified by the *msid* flag in the Master Source Observation Table). For these objects we chose the flux corresponding to the most sensitive observation. Since 2 observations overlapped the same pointing (ObsIDs 7823 and 9583), the deeper observation, ObsID 7823 at ~ 65 ks, was utilized, so effectively 94 individual pointings were used to construct the S82 ACX catalog. To avoid skewing our statistics and introducing a bias into our catalog, we also removed targeted observations from our source list, identified as the source within 5” of the user supplied RA and Dec for the target of the observation; we note that only 20 pointings from the 94 observations in this

³That is, we chose sources where the following flags were set to 0: *extent_code*, *sat_src_flag*, *streak_src_flag*, and where the pileup fraction was less than 10%. A source is considered extended (i.e., *extent_code* is set to 1) if the intrinsic source extent, found by deconvolving the local PSF from the observed source extent (parameterized as a rotated elliptical Gaussian), is inconsistent with a point source at the 90% confidence level. Only one source suffered from significant pileup (i.e., pileup fraction 25%) and was thus discarded from our source list.

analysis had sources that met this criterion and were subsequently removed. As mentioned previously, 29 pointings are from the XDEEP2 survey, and thus do not have targeted sources. For the remaining 45 observations, either the targeted object was not detected at the 4.5σ level or the observer supplied X-ray coordinates of the target were not well determined.

In total, we detect 1127 unique X-ray sources in Stripe 82 ACX, with 1118 detected in the full band, 774 sources detected in the soft band and 239 X-ray sources in the hard band at the 4.5σ level. Of these, 9 objects were detected in only the soft band and 321 were detected solely in the full band; none were detected in just the hard band. The relatively small number of significant X-ray sources in the hard band is likely due to the shallow depth of the majority of the observations: the lower signal-to-noise in shorter exposures more adversely affects high energies due to the decreasing number of photons detected at higher energies and the statistics of small numbers. Indeed, analysis on the full *Chandra* Source Catalog outside of the Stripe 82 region shows a higher percentage of sources with significant flux in the hard band, likely due to the greater number of observations with longer exposure times.

3. Stripe 82 ACX Number Counts

We present the number density of sources as a function of flux, the $\log N - \log S$ relation. The binned differential number counts are given by:

$$\frac{dN}{dS} = \frac{\sum_{i=1}^{i=n} \frac{1}{\Omega_i}}{\Delta S_j} \quad (3)$$

where n is the number of sources in bin j , Ω_i is the limiting sky coverage associated with the i th source and ΔS_j is the width of the flux bin. Here, we follow the prescription of Mateos et al. (2008) to calculate S_j , a weighted flux to represent the bin centroid:

$$S_j = \sum_{i=1}^{i=n} w_i \times S_i, w_i = \frac{\frac{1}{\Omega_i}}{\sum_{i=1}^{i=n} \frac{1}{\Omega_i}} \quad (4)$$

The error is given by Poissonian statistics:

$$\frac{dN/dS}{\sqrt{n}} \quad (5)$$

We have binned by 25, 10 and 40 sources in the soft, hard and full bands, respectively: each bin, except for the highest flux bin, have equal number of sources rather than equal energy widths.

In integral form, the cumulative source distribution is represented by:

$$N(> S) = \sum_{i=1}^{N_s} \frac{1}{\Omega_i} \quad (6)$$

where $N(>S)$ is the number of sources with a flux greater than S and Ω_i is defined as above. The associated error is the variance:

$$\sigma^2 = \sum_{i=1}^{N_s} \left(\frac{1}{\Omega_i}\right)^2 \quad (7)$$

The normalized representation of the Stripe 82 ACX $\text{Log}N$ - $\text{Log}S$ relationships (i.e., $dN/dS \times S_{14}^{2.5}$ and $N(>S) \times S_{14}^{1.5}$, where S_{14} is flux in units of $10^{-14} \text{ erg cm}^{-2} \text{ s}^{-1}$) are shown in Figure 5 as black circles, with the binned differential counts on the left and cumulative integral counts on the right. At the bright flux end, the Stripe 82 ACX number counts are Euclidean, as shown by the horizontal shape in this normalized representation.

We compare our number counts with previous X-ray surveys that span the range from deep, small area (ECDF-S, at 0.3 deg^2 with a soft band flux limit of $\sim 1.1 \times 10^{-16} \text{ erg cm}^{-2} \text{ s}^{-1}$, Lehmer et al. 2005), more moderate area, though still rather deep (*Chandra*-COSMOS at 0.9 deg^2 with a 0.5-2keV flux limit of $\sim 1.9 \times 10^{-16} \text{ erg cm}^{-2} \text{ s}^{-1}$, Elvis et al. 2009), moderate area, moderate depth (XDEEP2 at 3.2 deg^2 with a 0.5-2keV flux limit of $\sim 2 \times 10^{-16} \text{ erg cm}^{-2} \text{ s}^{-1}$, Goulding et al. 2012) and wide area and moderate depth (ChaMP, at 9.6 deg^2 and a soft band flux limit of $\sim 2.5 \times 10^{-16} \text{ erg cm}^{-2} \text{ s}^{-1}$, Kim et al. 2007b); only ChaMP has made differential number counts available for comparison. A comparison with the AGN number counts from the population synthesis models from Gilli et al. (2007) is also presented. We note that although the extended ChaMP/SDSS study has a greater survey area, it represents an optically selected QSO sample incorporating X-ray detections and flux limits, thus no X-ray $\text{Log}N$ - $\text{Log}S$ is published in that work. Stripe 82 ACX, however, considers all X-ray detected sources, regardless of whether or not an optical counterpart has yet been identified. ECDF-S, C-COSMOS and ChaMP adopt the same spectral model (absorbed power law with $\Gamma=1.4$) to estimate source flux while the XDEEP2 survey uses a spectral index of 1.7. Since the flux ranges for the comparison surveys differ in the hard (2-10 keV for C-COSMOS and the Gilli et al. (2007) model predictions, 2-8 keV for E-CDFS and ChaMP) and full (0.5-10 keV for C-COSMOS and 0.5-8 keV for ChaMP) bands from Stripe 82 ACX (2-7 keV and 0.5-7 keV, respectively), we have adjusted the values from previous surveys using the assumed spectral model of a power law with $\Gamma=1.4$ (i.e., we multiplied the comparison fluxes by factors of 0.68, 0.86, 0.76, and 0.91 respectively). Since the Stripe 82 ACX catalog only

includes sources with a flux significance exceeding 4.5σ , we do not see evidence of Eddington bias (promotion of spurious sources into the source list due to statistical fluctuations at the detection limit of each observation) which tends to steepen the source counts at the survey sensitivity limit.

In the soft and full bands, Stripe 82 ACX agrees with ECDF-S, C-COSMOS, XDEEP2 and the Gilli et al. (2007) model within the quoted error bars, and is slightly systematically lower than ChaMP (though consistent within the error bars), which has similar (or slightly better) sensitivity at high fluxes. The systematic offset in the hard band between Stripe 82 ACX and previous surveys and model predictions can be due to the shallow depth of the majority of observations in Stripe 82, which as noted above, decreases the signal-to-noise which in turn effects the higher energies more than the soft and full bands. We note that Stripe 82 ACX is incomplete at low fluxes due to the shallow to moderate depth covered by the majority of archival observations. Goulding et al. (2012) find the soft band $\log N$ - $\log S$ of the XDEEP2 survey, with half of whose pointings Stripe 82 ACX overlaps, to be systematically lower than ECDF-S and C-COSMOS at the high flux end (though consistent within the 90% confidence interval), which they attribute to higher completeness in XDEEP2 since they cover a greater ($\sim 3.2 \text{ deg}^2$) area. However, the high flux end of Stripe 82 ACX shows better agreement with E-CDFS and C-COSMOS than XDEEP2. The addition of another $\sim 13 \text{ deg}^2$ of archival and proprietary *XMM-Newton* X-ray coverage in Stripe 82 is expected to double the number of high flux X-ray sources and extend the $\log N$ - $\log S$ parameter space to higher flux values. In a future paper, with the benefit of streamlined multi-wavelength follow-up due to wealth of pre-existing data, we will quantify the impact of this population by generating the quasar luminosity function, beginning with the $\log N$ - $\log S$ distributions presented here.

4. Discussion

4.1. Deep Surveys vs. Wide Surveys: Probing a Unique Phase of Black Hole Growth

Spectroscopic redshifts, or well constrained photometric redshifts, are necessary to robustly calculate X-ray luminosities. The *Chandra* Source Catalog provides a matched catalog of X-ray sources with the Sloan Digital Sky Survey (SDSS) Data Release 7 (Abazajian et al. 2009). Details of the matching algorithm are described in Rots & Budavári (2011), where they use the Bayesian probabilistic algorithm presented in Budavári & Szalay (2008). In brief, for each possible association, a Bayes factor is calculated using a positional uncertainty of $0.1''$ for the SDSS sources and a varying error for *Chandra* sources based on the 95%

accuracy limit. A uniform prior is then assumed, which is a function of the number of X-ray and optical sources as well as the number of true pairs. All sources in the cross-matched catalog are those where the probability of a match exceeds 50%.

Six hundred twenty-three *Chandra* sources have optical counterparts in SDSS, 13 of which have two possible optical counterparts. We have verified these matches by visual inspection and have removed optical counterparts that are saturated, contaminated by proximity to a bright non-point source, are coincident with diffraction spikes and faint photometric sources from DR7 that do not have photometric detections in Data Release 8 (DR8). For the 13 X-ray objects with two possible optical counterparts, we chose the source with a higher probability of a match. This vetting leaves 609 matched X-ray and optical sources, which were matched with the following optical catalogs to find redshifts: SDSS DR8 (Aihara et al. 2011), SDSS-III (Eisenstein et al. 2011), 2SLAQ (Richards et al. 2005), WiggleZ (Drinkwater et al. 2010) and the 4th release of the DEEP2 catalog (Newman et al. 2012). We find spectroscopic redshifts for 277 X-ray sources, of which 259 have $L_x \geq 10^{42}$ erg s $^{-1}$ (where $L_x = L_{0.5-7\text{keV}}$), and are therefore likely AGN (e.g., Persic et al. 2004).

In Figure 6, we compare Stripe 82 ACX with a deep, narrow area survey, the MUSYC survey of CDF-S + E-CDFS (Cardamone et al. 2010), and C-COSMOS (Civano et al. 2012) to illustrate the advantage of larger areas in expanding the parameter space explored by pencil beam and moderate area surveys. Here we focus on the luminosity distributions for X-ray identified AGN at all spectroscopic redshifts and for the subset of sources where $z > 2$. Using the X-ray source list as the parent sample for both surveys, the spectroscopic completeness is comparable with CDF-s + E-CDFS: $\sim 24\%$ for Stripe 82 ACX and $\sim 28\%$ for CDF-S and ECDF-S (314 of 1134 X-ray sources have reliable spectroscopic redshifts, see Cardamone et al. 2010 for details); C-COSMOS has a higher level of spectroscopic completeness (48%). We note that the X-ray luminosities for Stripe 82 ACX and for CDF-S + E-CDFS are observed luminosities while the C-COSMOS luminosities have been k-corrected to the rest frame. It is immediately apparent that Stripe 82 ACX complements the deeper surveys by filling in the high X-ray luminosity parameter space, especially beyond $L_x \geq 3 \times 10^{44}$ erg s $^{-1}$: the Stripe 82 ACX luminosity distribution peaks where E-CDFS + CDF-S and C-COSMOS begins to taper off. C-COSMOS does find significantly more AGN at low to moderate luminosities, yet Stripe 82 ACX uncovers over twice as many systems beyond $\log(L_x)$ of 44.5 dex (115 vs. 57) prior to dedicated spectroscopic follow-up campaigns. At the peak of black hole growth ($z \sim 2$), only wider area surveys, like Stripe 82 ACX, locate rare $L_x > 10^{45}$ erg s $^{-1}$ quasars. Such objects provide a necessary probe of black hole growth and SMBH and host galaxy co-evolution models.

The largest number of X-ray selected $z > 3$ AGN from a contiguous survey was found

in C-COSMOS (Civano et al. 2011), with 81 spectroscopically confirmed high redshift AGN. Of the 119 optically selected $z > 3$ AGN in the Boötes field (Kochanek et al. 2012), 35 were detected in the XBoötes survey (Kenter et al. 2005). Based on population synthesis models from Treister et al. (2009), ~ 1000 $z > 3$ AGN are predicted to lie in 20 deg^2 above the survey flux limits, assuming a soft band flux limit of $7.9 \times 10^{-16} \text{ erg s}^{-1} \text{ cm}^{-2}$ for 7.5 deg^2 of *Chandra* coverage (see Table 1) and $2 \times 10^{-15} \text{ erg s}^{-1} \text{ cm}^{-2}$ for 12 deg^2 of *XMM-Newton* coverage (approximate flux limit of a 15 ks observation). When folding in the area-flux curve, we expect to identify about an order of magnitude fewer AGN in this redshift range, as comparisons between the predicted AGN numbers using the observed soft band area-flux curve and the number above the survey flux limit differ by approximately this amount. The population synthesis model from Gilli et al. (2007), which applies an exponential decline to the high redshift AGN space density (see, e.g., Civano et al. 2011), predicts half the number of AGN compared with Treister et al. (2009)’s model. The Stripe 82 X survey will give us an opportunity to test these model predictions. In Stripe 82 ACX, a total of 4 $z > 3$ AGN have been spectroscopically confirmed so far. In Figure 7, we show an example of such a high redshift ($z = 3.62$), high luminosity ($L_x = 3.8 \times 10^{45} \text{ erg s}^{-1}$) quasar, the most distant source in our sample. We downloaded the X-ray spectrum and associated response files from the *Chandra Source Catalog* for this source (CXO J022518.1-001332), with coordinates RA = 36.32, Dec = -0.226. As can be seen in Figure 7 (a), enough net counts (~ 265) were detected in the full band for a model to be fitted to the spectrum, overplotted in red. Here we binned the spectrum by a minimum of 25 counts per bin and used an absorbed power law, with the absorption fixed to the Galactic value ($N_H = 2.9 \times 10^{20} \text{ cm}^{-2}$). The best-fit power law index is $\Gamma = 1.63_{-0.24}^{+0.25}$, which gives an observed full band (0.5-7 keV) luminosity of $2.8 \times 10^{45} \text{ erg s}^{-1}$, largely consistent with the estimate based on our assumed spectral model to convert from count rate to energy flux. Panel (b) of Figure 7 shows the optical spectrum from SDSS (SDSS J022518.36-001332.3), with the SDSS-III best fit template spectrum from the *spec1d* pipeline (Bolton et al. 2012) overplotted in red. Prominent emission lines of Ly α , NV, SiIV and CIV are clearly visible.

4.2. Obscured AGN

Five hundred eighteen X-ray sources do not have optical counterparts in SDSS. We have reviewed the optical images by eye and find that a handful of these fields are contaminated by extended emission from a saturated star, but the vast majority are true non-detections. SDSS easily detects Type 1 (unobscured) quasars, which swamp out the emission of their host galaxies, out to high redshifts ($z > 5$), but L_* galaxies, where Type II (obscured) AGN are likely to live, fall below the detectability threshold at $z \sim 1$. At the average depth of

Stripe 82 ACX, X-rays allow us to peer deeper into the cosmos than optical light, so these X-ray sources are candidate obscured AGNs and obscured quasars in the distant Universe. Matching these SDSS non-detections with the UKIDSS catalog using the maximum likelihood estimation matching algorithm from Brusa et al. (2007) as implemented in the MUSYC survey (Cardamone et al. 2010), we find 17 and 39 X-ray sources detected in the J and K bands, respectively, making them high redshift, obscured AGN candidates. In a future paper, when we release the full ~ 20 deg² Stripe 82 X Catalog and multi-wavelength data, we will discuss such objects in greater detail.

In the local universe ($z < 0.5$), Type 2 AGN can be optically identified using the diagnostic BPT diagram (Baldwin et al. 1981); beyond this distance, H α is redshifted out of the rest-frame optical bandpass. Of the 259 X-ray identified AGN in Stripe 82 ACX, 212 have spectra showing broad emission lines and are therefore Type 1 AGN. Forty-four objects are optically classified as galaxies and the 3 remaining sources have spectroscopic redshifts from the WiggleZ survey (which provides redshift information, but not spectroscopic type; their optical identifications as galaxies or quasars are therefore undetermined). Of the 40 X-ray identified AGN with “galaxy” type spectra, 34 are at $z \leq 0.5$ where we can use the BPT diagram to identify Seyfert 2 galaxies (Sy2s, local obscured AGN) and composite systems (galaxies which appear to have comparable amounts of star-formation activity as well as accretion onto a central SMBH).

Focusing on all X-ray detected sources that are optically classified as “galaxies,” regardless of whether their X-ray luminosity exceeds 10^{42} erg s^{−1}, 36 of the 45 objects below $z = 0.5$ have optical spectra where the emission line fluxes could be well fitted. In Figure 8, we plot their [OIII] λ 5007/H β and [NII] λ 6583/H α ratios on the BPT diagram to compare optical and X-ray identifications of AGN. The X-ray identified AGN ($L_x > 10^{42}$ erg s^{−1}) are marked by red circles, whereas black diamonds indicate the sources that do not meet this threshold. The upper dotted line represents the Kewley et al. (2001) theoretical maximum starburst line: any source above this line is a Sy2 or a LINER (low-ionization nuclear emission line region, with the empirical dividing line between the two classes derived from Schawinski et al. (2007) shown by the solid line). The dashed line illustrates the empirical dividing line between star-forming galaxies and composites from Kauffmann et al. (2003). As shown in Figure 8, X-ray selection identifies AGN in all regions of this parameter space, similar to the findings of previous X-ray sources, such as C-COSMOS (Civano et al. 2012), *XMM-COSMOS*, (Bongiorno et al. 2010) and OPTX (Trouille et al. 2011). The two optically identified star-forming galaxies in this sample have moderate X-ray luminosities ($L_x = 1.4 \times 10^{43}$ and 4.2×10^{43} erg s^{−1}), and are thus likely host galaxy obscured AGN: that is, large amounts of dust attenuates the optical signatures of SMBH accretion yet X-rays can easily pierce through this obscuration. In addition, 7 optically detected Sy2s and 3

composite galaxies have X-ray luminosities below the canonical $L_x=10^{42}$ erg s $^{-1}$ definition. This is not unexpected because many AGN have luminosities lower than 10^{42} erg s $^{-1}$; this cut is used simply to reduce contamination of the AGN sample by star-forming galaxies, not because this is a lower bound to AGN luminosities.

All X-ray identified AGN residing in systems optically classified as galaxies have low to moderate X-ray luminosities, 10^{42} erg s $^{-1} < L_x < 10^{44}$ erg s $^{-1}$. To test whether the optically identified Sy2s and composites have intrinsically weak X-ray emission or if the X-rays are attenuated, we have calculated the ratio of L_x to the observed [OIII] luminosity ($L_{[OIII]}$); this ratio has been shown to be a reliable estimate of “toroidal” obscuration in Sy2s since the X-ray emission is absorbed by the torus while the [OIII] line forms in the Narrow Line Region and is thus unaffected by toroidal absorption (Bassani et al. 1999; Heckman et al. 2005; Cappi et al. 2006; Panessa et al. 2006; LaMassa et al. 2009, 2011). In such analyses, the hard band (2-10 keV) flux, rather than the full band, is often used. However, due to the few significant flux detections in the hard band, here we use the broad band luminosity. The distribution of $L_x/L_{[OIII]}$ is shown in Figure 9, with the grey shaded region indicating the average value for unobscured Seyfert 1 galaxies ($\text{Log} (L_{2-10\text{keV}}/L_{[OIII]}) = 1.59 \pm 0.49$ dex) from a heterogeneously selected [OIII]-bright sample presented in Heckman et al. (2005). For X-ray sources in Stripe 82 ACX with significant hard band detections, the ratio of $F_{\text{broad}}/F_{\text{hard}}$ generally ranges from 0.6 to 2, with the largest outlier at 5.0. Thus we do not expect systematic biases introduced by comparing $L_{0.5-7\text{keV}}/L_{[OIII]}$ to the average Seyfert 1 $L_{2-10\text{keV}}/L_{[OIII]}$ values. A majority of these Sy2s and composites have $L_x/L_{[OIII]}$ values consistent with, or higher than, those observed for unobscured AGN, suggesting that the observed X-ray emission is not attenuated. This result is not surprising considering this sample is X-ray selected, which favors unobscured AGN in the local Universe. These low to moderate X-ray luminosities then likely reflect the intrinsic X-ray emission. This also means survey areas considerably larger than 7.5 deg 2 are needed to probe the highest luminosity AGN. The three sources with $\text{Log} (L_x/L_{[OIII]}) < 1$ dex are above the canonical X-ray luminosity AGN definition, albeit at low luminosities (i.e., $L_x < 3 \times 10^{42}$ erg s $^{-1}$); these objects are likely obscured by a substantial amount of gas associated with the torus and may potentially be Compton-thick candidates.

4.3. AGN Predictions

Using the population synthesis models from Treister et al. (2009) and Gilli et al. (2007), we can predict the expected AGN luminosity distribution. Given the observed full band 0.5-7 keV area-flux curve in Stripe 82 ACX (Figure 4), the dot-dashed blue line in Figure 10

represents the AGN we can expect to uncover with additional spectroscopic redshifts and tightly constrained photometric redshifts. We also show the expected luminosity distributions from full SDSS Stripe 82 area coverage (300 deg²) in X-rays, as well as an intermediate area coverage of 100 deg², assuming a full band flux limit of 1×10^{-14} erg cm⁻² s⁻¹, the approximate flux limit of a 15 ks exposure with *Chandra*. Both models predict that an investment in X-ray coverage over a substantial fraction of the Stripe 82 region, even at 100 deg², with its substantial pre-existing multi-wavelength coverage, will provide a major advance in describing the luminous fraction of black hole growth that is currently not well measured.

5. Conclusion

We have presented the first 7.5 deg² of the current 20 deg² X-ray survey covering SDSS Stripe 82. The present work concerns the analysis of archival *Chandra* observations in the region (Stripe 82 ACX). We utilized source lists and products generated and provided by the *Chandra* Source Catalog (Evans et al. 2010), and the extensive multiwavelength data available in Stripe 82, which greatly streamlined the analysis compared with previous X-ray surveys. Our main results are summarized as follows:

- Stripe 82 ACX reaches down to approximate flux limits of 7.9×10^{-16} , 3.4×10^{-15} and 1.8×10^{-15} erg s⁻¹ cm⁻², with half area survey coverage at fluxes of 1.4×10^{-14} , 4.7×10^{-14} and 2.8×10^{-14} erg s⁻¹ cm⁻², in the soft (0.5-2 keV), hard (2-7 keV) and full (0.5-7 keV) bands, respectively. We detect a total of 1127 unique X-ray sources, with 774, 239 and 1118 sources at the 4.5 σ level in the soft, hard and full bands. Of these, 321 were detected solely in the full band and 9 sources detected only in the soft band.
- Our soft and full band Log N -Log S relations are consistent with the predictions from Gilli et al. (2007) and previous *Chandra* X-ray surveys: ECDF-S (Lehmer et al. 2005), C-COSMOS (Elvis et al. 2009), XDEEP2 (Goulding et al. 2012) and ChaMP (Kim et al. 2007b). The slight systematic disagreement in the hard band fluxes is likely due the shorter exposure times in Stripe 82 ACX, where the lower signal-to-noise adversely affects higher energies. The number counts for Stripe 82 ACX are Euclidean at high fluxes.
- 609 *Chandra* sources are matched to optical counterparts in the SDSS. We obtained spectroscopic redshifts for 277 of these X-ray objects from SDSS DR8 (Aihara et al. 2011), SDSS-III (Eisenstein et al. 2011), 2SLAQ (Richards et al. 2005), WiggleZ (Drinkwater et al.

2010) and DEEP2 (Newman et al. 2012). Two hundred fifty-nine of these objects have X-ray luminosities consistent with AGN (i.e. $L_x \geq 10^{42}$ erg s $^{-1}$).

- We compared the luminosity distributions of AGN from Stripe 82 ACX with CDF-S + E-CDFS (Cardamone et al. 2010) and C-COSMOS (Civano et al. 2012); E-CDFS + CDF-S has similar level of spectroscopic completeness with Stripe 82 ACX when considering the X-ray catalog as the parent sample, while C-COSMOS has a much higher level of spectroscopic completeness. This comparison shows that the wider area probed, even at the modest level presented here, improves the census of the high luminosity (i.e., $L_x > 3 \times 10^{44}$ erg s $^{-1}$) AGN population, especially at $z > 2$. Stripe 82 ACX peaks in luminosity where CDF-S + E-CDFS tapers off and finds double the number of sources at high luminosities than C-COSMOS.
- Using the optical BPT diagram (Baldwin et al. 1981) for the 36 optically classified galaxies with spectra where the appropriate emission lines could be well fitted, we confirm that X-ray selection identifies AGN that live in the Seyfert 2, composite and star-forming loci. The galaxies optically classified as star-forming galaxies have moderate X-ray luminosities, suggesting that host galaxy obscuration suppresses optical signatures of AGN activity, but not the X-ray flux. Conversely, optical identification locates 7 Sy2s and 3 composite systems lie below the X-ray luminosity AGN cut applied in order to obtain pure X-ray selected samples of AGN.
- We have used the ratio of $L_x/L_{[OIII]}$ as a diagnostic of toroidal obscuration (e.g. Heckman et al. 2005; LaMassa et al. 2009, 2011) and find that a majority of optically identified Sy2s and composites do not exhibit evidence of obscuration. The low to moderate X-ray luminosities in these sources thus likely represent the intrinsic X-ray emission.
- Using population synthesis models from Treister et al. (2009) and Gilli et al. (2007), we have predicted the redshift and luminosity distributions of AGN we can expect to observe in the current 7.5 deg 2 , 100 deg 2 and 300 deg 2 (the full area of SDSS Stripe 82). In order to fully utilize the advantage of a wide area X-ray survey, multi-wavelength data are essential for accurate redshifts through either optical spectroscopy or well constrained photometric data, making Stripe 82 an ideal location for a wider area X-ray survey.

REFERENCES

Abazajian, K. N., Adelman-McCarthy, J. K., Agüeros, M. A., et al. 2009, ApJS, 182, 543

- Aihara, H., Allende Prieto, C., An, D., et al. 2011, *ApJS*, 193, 29
- Alexander, D. M., Bauer, F. E., Brandt, W. N., et al. 2003, *AJ*, 126, 539
- Baldwin, J. A., Phillips, M. M., & Terlevich, R. 1981, *PASP*, 93, 5
- Bassani, L., Dadina, M., Maiolino, R., et al. 1999, *ApJS*, 121, 473
- Becker, R. H., White, R. L., & Helfand, D. J. 1995, *ApJ*, 450, 559
- Bolton, A. S., Schlegel, D. J., Aubourg, E., et al. 2012, *arXiv:1207.7326*
- Bongiorno, A., Mignoli, M., Zamorani, G., et al. 2010, *A&A*, 510, A56
- Brusa, M., Zamorani, G., Comastri, A., et al. 2007, *ApJS*, 172, 353
- Budavári, T., & Szalay, A. S. 2008, *ApJ*, 679, 301
- Cappelluti, N., Brusa, M., Hasinger, G., et al. 2009, *A&A*, 497, 635
- Cappi, M., Panessa, F., Bassani, L., et al. 2006, *A&A*, 446, 459
- Cardamone, C. N., van Dokkum, P. G., Urry, C. M., et al. 2010, *ApJS*, 189, 270
- Civano, F., Elvis, M., Brusa, M., et al. 2012, *arXiv:1205.5030*
- Civano, F., Brusa, M., Comastri, A., et al. 2011, *ApJ*, 741, 91
- Comastri, A., Ranalli, P., Iwasawa, K., et al. 2011, *A&A*, 526, L9
- Das, S., Marriage, T. A., Ade, P. A. R., et al. 2011, *ApJ*, 729, 62
- Drinkwater, M. J., Jurek, R. J., Blake, C., et al. 2010, *MNRAS*, 401, 1429
- Eisenstein, D. J., Weinberg, D. H., Agol, E., et al. 2011, *AJ*, 142, 72
- Elvis, M., Civano, F., Vignali, C., et al. 2009, *ApJS*, 184, 158
- Elyiv, A., Clerc, N., Plionis, M., et al. 2012, *A&A*, 537, A131
- Emerson, J., & Sutherland, W. 2010, *The Messenger*, 139, 2
- Evans, I. N., Primini, F. A., Glotfelty, K. J., et al. 2010, *ApJS*, 189, 37
- Gawiser, E., van Dokkum, P. G., Herrera, D., et al. 2006, *ApJS*, 162, 1
- Gialalisco, M., Ferguson, H. C., Koekemoer, A. M., et al. 2004, *ApJ*, 600, L93

- Gilli, R., Comastri, A., & Hasinger, G. 2007, *A&A*, 463, 79
- Goulding, A. D., Forman, W. R., Hickox, R. C., et al. 2012, arXiv:1206.6884
- Green, P. J., Aldcroft, T. L., Richards, G. T., et al. 2009, *ApJ*, 690, 644
- Hasinger, G., Cappelluti, N., Brunner, H., et al. 2007, *ApJS*, 172, 29
- Heckman, T. M., Ptak, A., Hornschemeier, A., & Kauffmann, G. 2005, *ApJ*, 634, 161
- Hodge, J. A., Becker, R. H., White, R. L., Richards, G. T., & Zeimann, G. R. 2011, *AJ*, 142, 3
- Kauffmann, G., Heckman, T. M., Tremonti, C., et al. 2003, *MNRAS*, 346, 1055
- Kenter, A., Murray, S. S., Forman, W. R., et al. 2005, *ApJS*, 161, 9
- Kewley, L. J., Dopita, M. A., Sutherland, R. S., Heisler, C. A., & Trevena, J. 2001, *ApJ*, 556, 121
- Kim, M., Kim, D.-W., Wilkes, B. J., et al. 2007a, *ApJS*, 169, 401
- Kim, M., Wilkes, B. J., Kim, D.-W., et al. 2007b, *ApJ*, 659, 29
- Kochanek, C. S., Eisenstein, D. J., Cool, R. J., et al. 2012, *ApJS*, 200, 8
- Laird, E. S., Nandra, K., Georgakakis, A., et al. 2009, *ApJS*, 180, 102
- LaMassa, S. M., Heckman, T. M., Ptak, A., et al. 2011, *ApJ*, 729, 52
- LaMassa, S. M., Heckman, T. M., Ptak, A., et al. 2009, *ApJ*, 705, 568
- Lawrence, A., Warren, S. J., Almaini, O., et al. 2007, *MNRAS*, 379, 1599
- Lehmer, B. D., Brandt, W. N., Alexander, D. M., et al. 2005, *ApJS*, 161, 21
- Martin, D. C., Fanson, J., Schiminovich, D., et al. 2005, *ApJ*, 619, L1
- Mateos, S., Warwick, R. S., Carrera, F. J., et al. 2008, *A&A*, 492, 51
- Murray, S. S., Kenter, A., Forman, W. R., et al. 2005, *ApJS*, 161, 1
- Newman, J. A., Cooper, M. C., Davis, M., et al. 2012, arXiv:1203.3192
- Panessa, F., Bassani, L., Cappi, M., et al. 2006, *A&A*, 455, 173
- Persic, M., Rephaeli, Y., Braitto, V., et al. 2004, *A&A*, 419, 849

- Pierre, M., Valtchanov, I., Altieri, B., et al. 2004, *J. Cosmology Astropart. Phys.*, 9, 11
- Primini, F. A., Houck, J. C., Davis, J. E., et al. 2011, *ApJS*, 194, 37
- Puccetti, S., Vignali, C., Cappelluti, N., et al. 2009, *ApJS*, 185, 586
- Reyes, R., Zakamska, N. L., Strauss, M. A., et al. 2008, *AJ*, 136, 2373
- Richards, G. T., Strauss, M. A., Fan, X., et al. 2006, *AJ*, 131, 2766
- Richards, G. T., Croom, S. M., Anderson, S. F., et al. 2005, *MNRAS*, 360, 839
- Rots, A. H., & Budavári, T. 2011, *ApJS*, 192, 8
- Schawinski, K., Thomas, D., Sarzi, M., et al. 2007, *MNRAS*, 382, 1415
- Scoville, N., Aussel, H., Brusa, M., et al. 2007, *ApJS*, 172, 1
- Treister, E., Urry, C. M., & Virani, S. 2009, *ApJ*, 696, 110
- Treister, E., Urry, C. M., Chatzichristou, E., et al. 2004, *ApJ*, 616, 123
- Trichas, M., Green, P. J., Silverman, J. D., et al. 2012, *ApJS*, 200, 17
- Trouille, L., Barger, A. J., & Tremonti, C. 2011, *ApJ*, 742, 46
- Trouille, L., Barger, A. J., Cowie, L. L., Yang, Y., & Mushotzky, R. F. 2008, *ApJS*, 179, 1
- Virani, S. N., Treister, E., Urry, C. M., & Gawiser, E. 2006, *AJ*, 131, 2373
- Xue, Y. Q., Luo, B., Brandt, W. N., et al. 2011, *ApJS*, 195, 10
- Yang, Y., Mushotzky, R. F., Steffen, A. T., Barger, A. J., & Cowie, L. L. 2004, *AJ*, 128, 1501

Table 1. Energy Band Summary

Band	Energy Range	Conversion Factors ¹ 10 ⁻⁹ erg/cm ² /s/photon	Number of Sources	Flux Limit erg/s/cm ²	Depth of half survey area erg/s/cm ²
Soft	0.5-2 keV	1.67	774	7.9×10 ⁻¹⁶	1.4×10 ⁻¹⁴
Hard	2-7 keV	6.08	239	3.4×10 ⁻¹⁵	4.7×10 ⁻¹⁴
Full	0.5-7 keV	3.31	1118	1.8×10 ⁻¹⁵	2.8×10 ⁻¹⁴

¹Based on absorbed power law model with $N_H = 3 \times 10^{20} \text{ cm}^{-2}$ and $\Gamma=1.4$

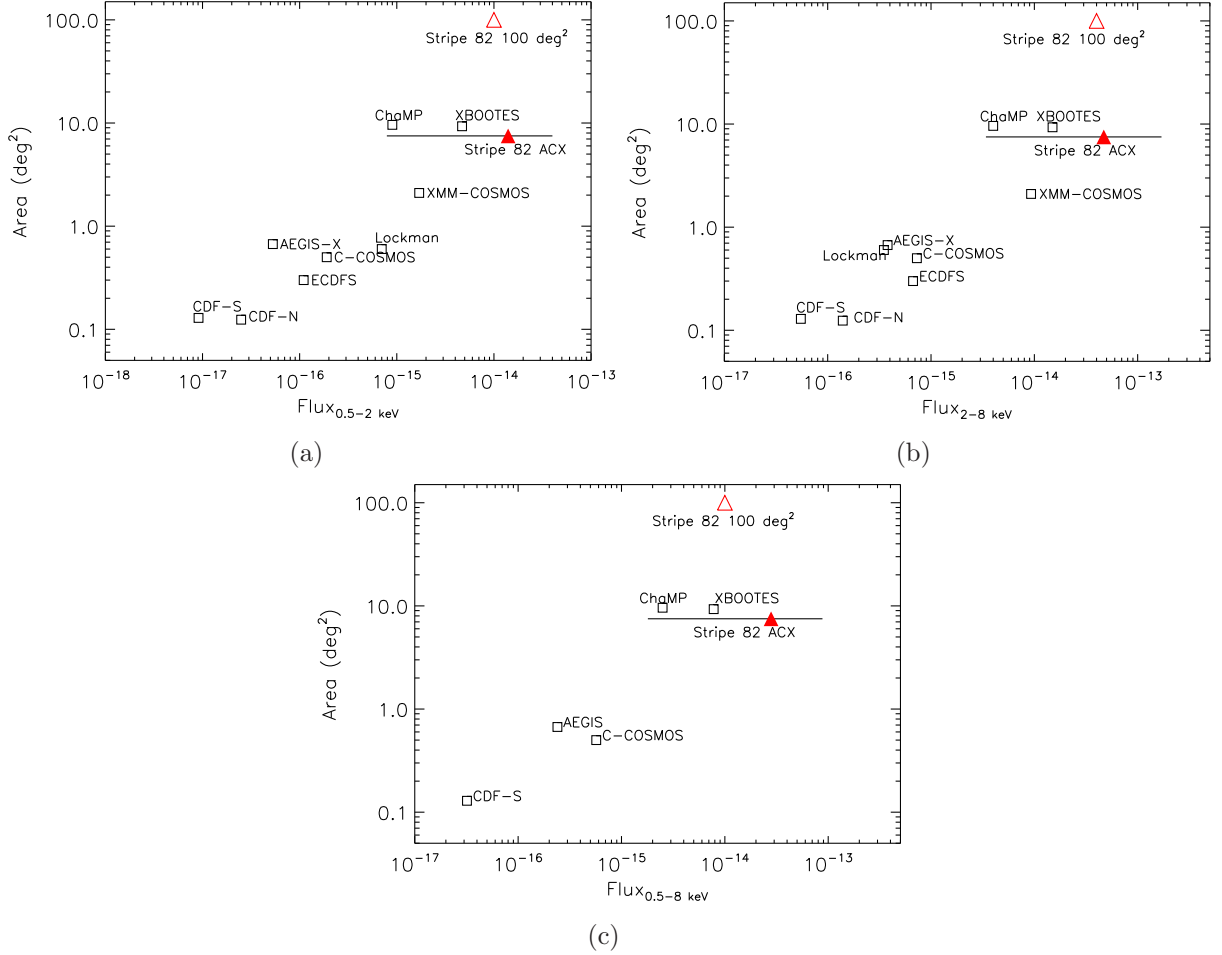


Fig. 1.— Comparison of area vs. flux in the soft band (a), hard band (b) and full band (c) for previous X-ray surveys and Stripe 82 ACX, with deepest flux and flux at full sky coverage shown by the horizontal line and the red triangle illustrating the flux limit at half area survey coverage. The empty red triangle illustrates the approximate flux limits with a *Chandra* exposure time of 15 ks for a 100 deg² survey in Stripe 82. The flux limits shown for the comparison surveys represents the deepest flux limit for on-axis pointing; with increasing off-axis distance ($\gtrsim 10''$), the depth becomes less sensitive by about an order of magnitude.

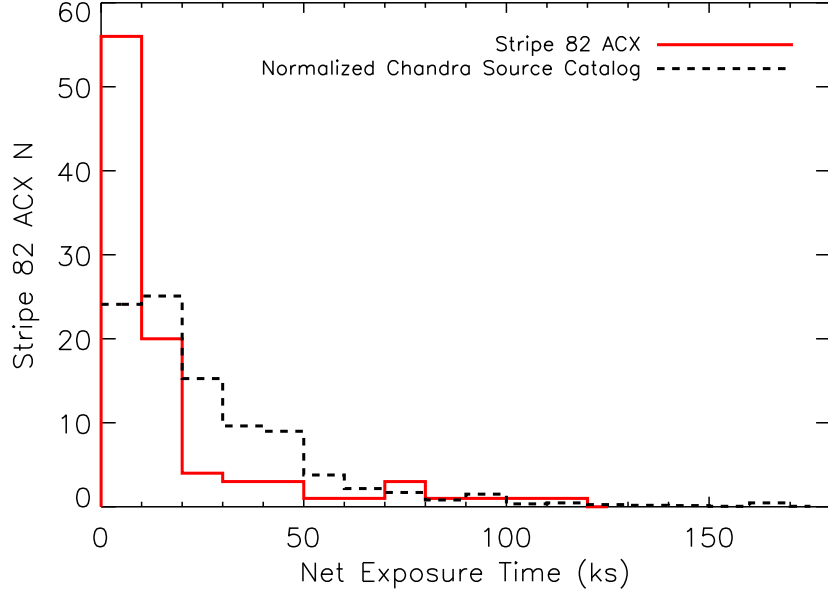


Fig. 2.— Distribution of exposure times for observations included in Stripe 82 ACX (red solid line) and for all ACIS observations (black dashed line) in the full *Chandra* Source Catalog with exposure time greater than 5 ks that are not in Stripe 82. The distribution for the *Chandra* Source Catalog is normalized by the number of sources in Stripe 82 ACX for ease of comparison. Stripe 82 has a significant fraction of more shallow observations than the general catalog.

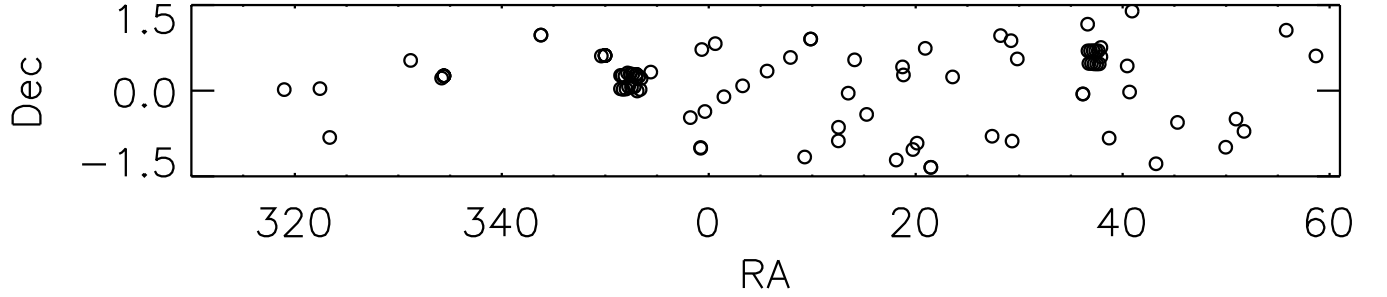


Fig. 3.— Locations of archival *Chandra* observations in Stripe 82. The dense cluster of pointings at $RA \approx 352^\circ$ and $RA \approx 37^\circ$ are Fields 3 and 4, respectively, of the XDEEP2 Survey (see Goulding et al. 2012, for details, including catalog of X-ray sources and optical counterparts).

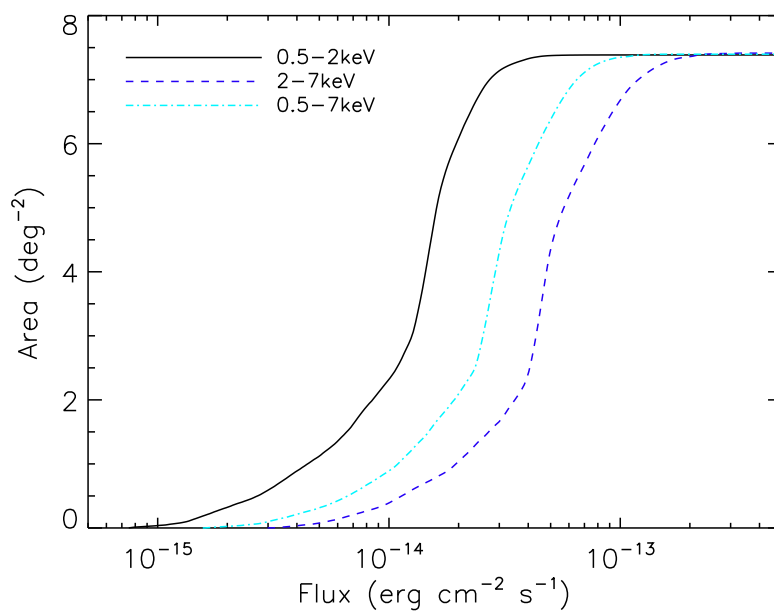


Fig. 4.— Stripe 82 ACX survey area as a function of limiting flux for the soft (0.5-2 keV, solid dark line), hard (2-7 keV, dashed blue line) and full (0.5-7 keV, dotted dashed cyan line) energy bands. Details concerning the derivation of these curves are given in the text.

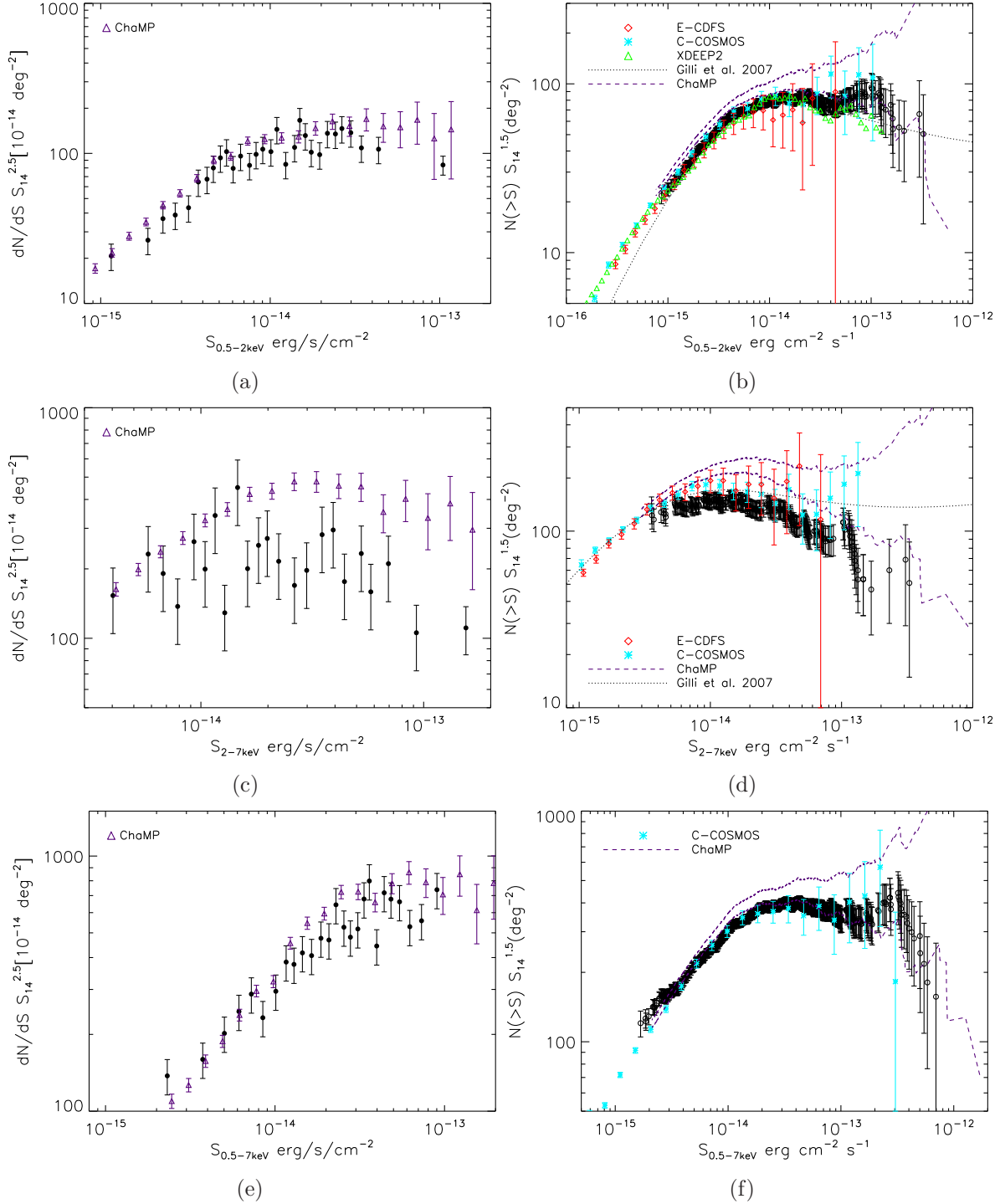


Fig. 5.— Normalized representation of the differential (left) and cumulative (right) number density of X-ray sources as a function of flux for Stripe 82 ACX (filled black circles) compared with the Extended *Chandra* Deep Field South (E-CDFS, red diamonds, Lehmer et al. 2005), *Chandra* COSMOS (C-COSMOS, cyan asterisks, Elvis et al. 2009), XDEEP2 (green triangles, Goulding et al. 2012) and ChaMP (purple triangles (left), 1σ confidence interval shown in the purple dashed line (right), Kim et al. 2007b) for the soft (top), hard (middle) and full (bottom) X-ray bands. The dotted line shows the predicted $\log N$ - $\log S$ from the Gilli et al. (2007) model. See text for discussion.

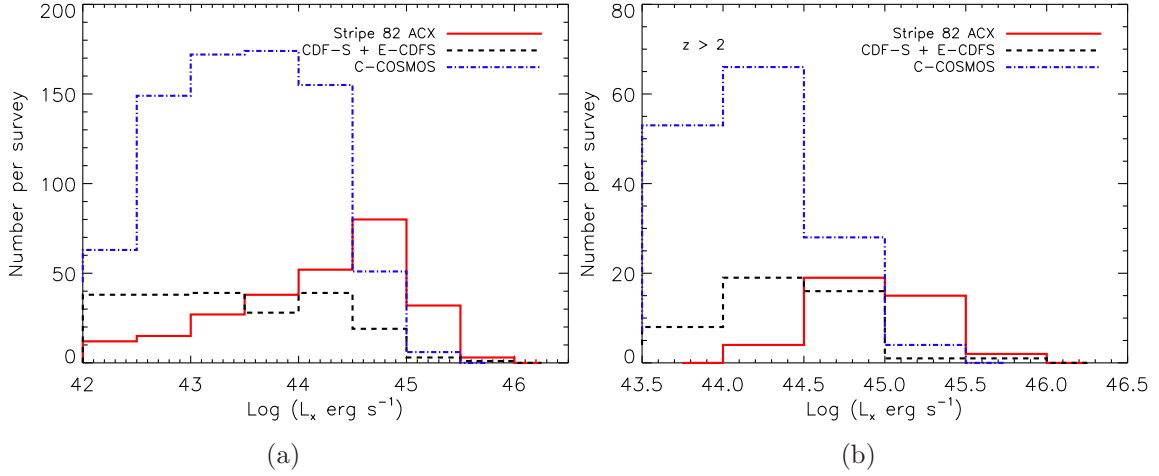


Fig. 6.— Luminosity distributions of AGN (i.e., X-ray sources with luminosities exceed $10^{42} \text{ erg s}^{-1}$) in Stripe 82 ACX (red solid line) compared with E-CDFS + CDF-S (black dashed line) and C-COSMOS (blue dot-dashed line) for all X-ray sources with spectroscopic redshifts (a) and with $z > 2$ (b). The advantage of wide area over deep, smaller area surveys in isolating high luminosity AGN is apparent, especially at high redshift. Though C-COSMOS finds significantly more sources at moderate luminosities, Stripe 82 ACX locates over twice the number of AGN at $\text{log}(L_x) > 44.5$ dex prior to a targeted spectroscopic follow-up campaign. As more area is added to the Stripe 82 X survey, this advantage will be enhanced.

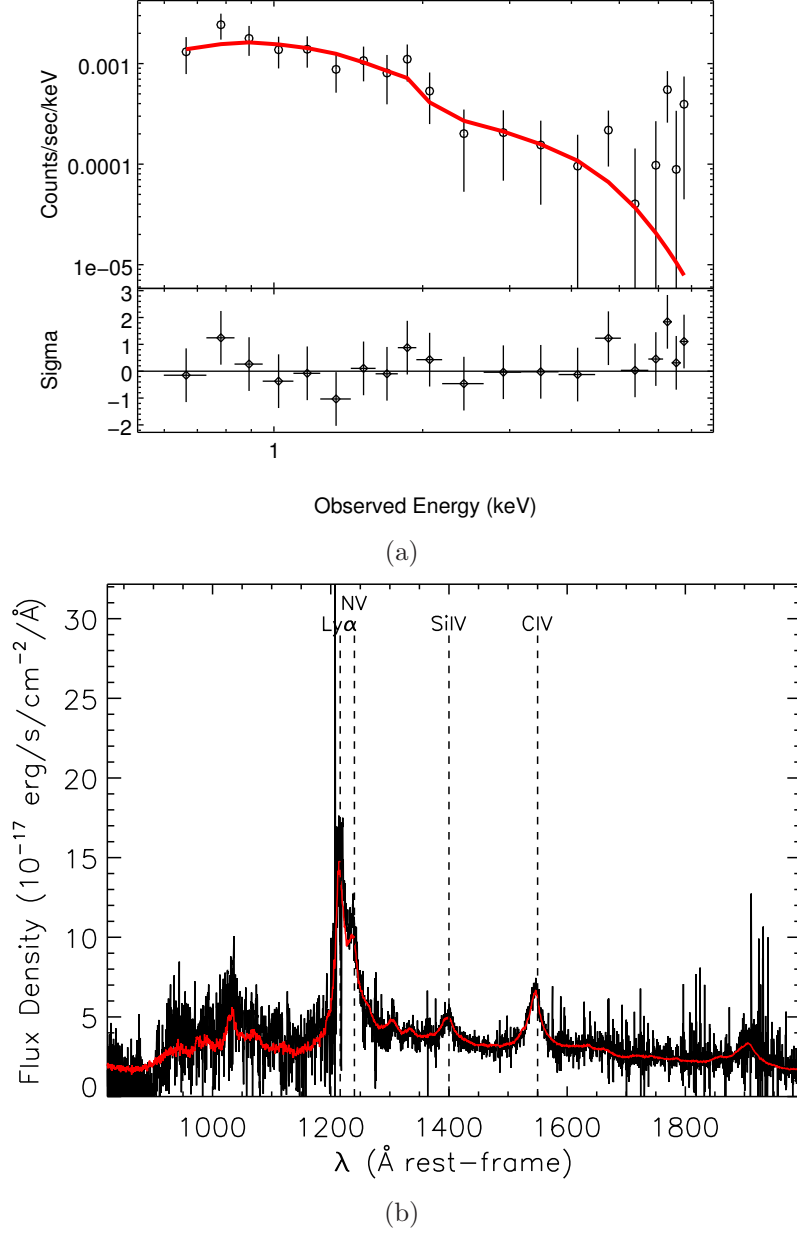


Fig. 7.— X-ray (a) and optical (b) spectra of a high redshift ($z = 3.62$), high luminosity ($L_x = 3.8 \times 10^{45}$ erg s $^{-1}$) quasar detected in Stripe 82 ACX. We fitted the X-ray spectrum with an absorbed power law model, overplotted in red, with N_H frozen to the Galactic value of 2.9×10^{20} cm $^{-2}$ and $\Gamma = 1.63^{+0.25}_{-0.24}$. In panel (b), we show the rest-frame SDSS-III spectrum of this source with the best-fit template spectrum from the *spec1d* pipeline (Bolton et al. 2012) overplotted in red. Prominent emission lines are identified as Ly α , NV, SiIV and CIV.

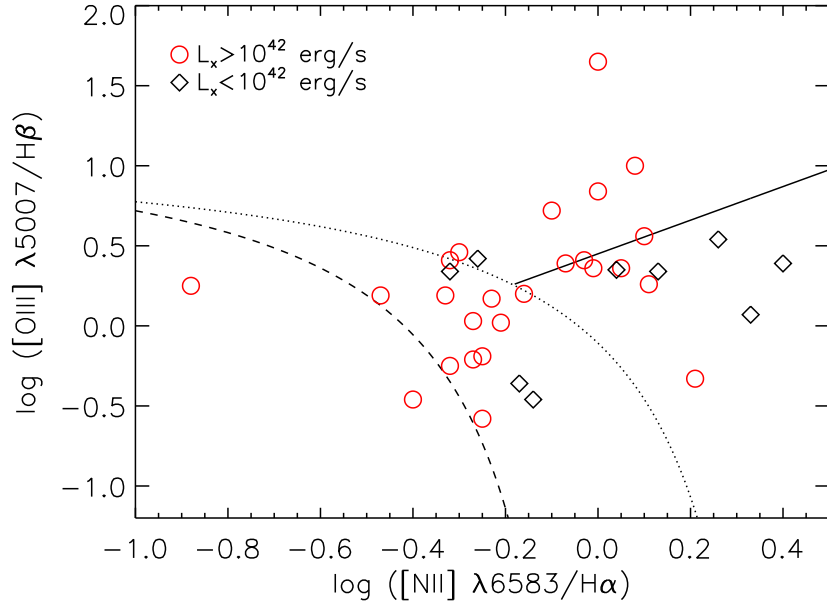


Fig. 8.— Optical BPT diagram (Baldwin et al. 1981) which differentiates between Sy2 galaxies, above the dotted line (Kewley et al. 2001); composites, between the dotted and dashed lines (Kauffmann et al. 2003); and star-forming galaxies, below the dashed line. The Schawinski et al. (2007) empirical demarcation between Sy2s and LINERS is shown by the solid line. X-ray identified AGN, i.e. those sources with X-ray luminosities exceeding $10^{42} \text{ erg s}^{-1}$, are marked by the red circles, while the objects with X-ray luminosities below this threshold are indicated by the black diamonds. X-ray identification locates AGN in all regions of this parameter space.

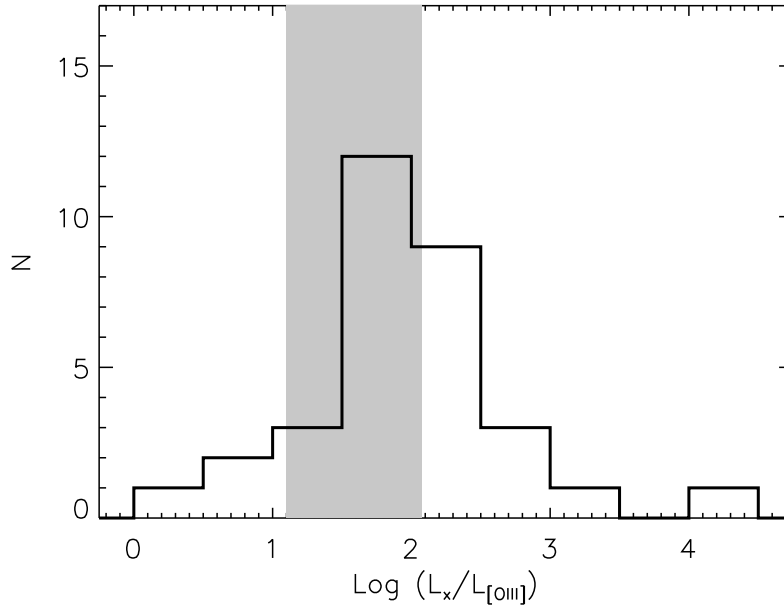


Fig. 9.— Distribution of $\text{Log} (L_x/L_{[OIII]})$, a reliable obscuration diagnostic, for optically identified Sy2s and composites. The gray shaded region shows the range for unobscured Seyfert 1 galaxies (Heckman et al. 2005). Only a small fraction of the AGN, below the Seyfert 1 values, show evidence for X-ray attenuation.

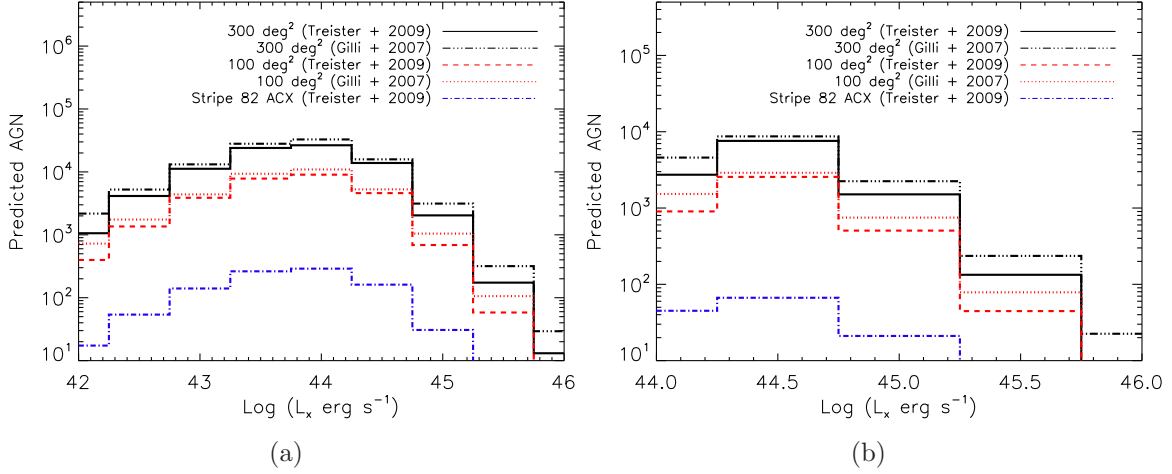


Fig. 10.— Predicted luminosity distributions of AGN (i.e., X-ray sources with luminosities exceed 10^{42} erg s^{-1}) using population synthesis models of Treister et al. (2009) for Stripe 82 ACX (blue dotted-dashed curve), given the observed area flux curve; and using models from Treister et al. (2009) and Gilli et al. (2007) for 100 deg² of Stripe 82 and if the full area of Stripe 82 (300 deg²) is covered in X-rays, assuming a full band flux limit of 1×10^{-14} erg cm^2 s^{-1} , the approximate depth of a 15 ks *Chandra* observation. Panel (a) is for all redshifts whereas panel (b) is for the subset of sources with $z > 2$. Not only is a wide area of X-ray coverage necessary to more fully explore the high redshift ($z > 2$) and high luminosity ($L > 10^{44}$ erg s^{-1}) regime, but multi-wavelength data, such as that existing in Stripe 82, are essential to accurately constrain the redshifts, and thus luminosities, of the X-ray detected sources.